mathematics

MDPI

Article

Investigating Behavior of Slider–Crank Mechanisms with Bearing Failures Using Vibration Analysis Techniques

Mofareh Hassan Ghazwani [1] and Van Vinh Pham [2,*]

[1] Department of Mechanical Engineering, Jazan University, P.O. Box 114, Jazan 45142, Saudi Arabia
[2] Institute of Energy & Mining Mechanical Engineering, Nha Trang 57100, Vietnam
* Correspondence: phamvv1978.iemm@gmail.com

Abstract: This study focuses on investigating the behavior of slider–crank mechanisms with different bearing failures using a vibration analysis technique. The reliability and lifespan of bearings are crucial for such mechanisms, which convert rotary motion to reciprocating motion. Previous research primarily addressed ball-bearing failures, neglecting needle bearings due to their specific applications. To bridge this gap, our experimental setup integrated both roller and ball bearings within a slider–crank mechanism. Vibration data were collected during normal operation, as well as under failure conditions of the ball and roller bearings. By analyzing the vibration signatures during simultaneous multiple failures, we gained insights into the nature of vibrations in the system. Furthermore, a mathematical model based on Hertzian contact was employed to calculate the theoretical frequency of ball bearings; however, due to the variable motion of the needle bearing, a novel mathematical model was proposed to estimate the defective impulse frequency, considering the inter-impact time between two impacts. The experimental results were compared with the healthy crank mechanism setup to draw meaningful conclusions. This research contributes to a comprehensive understanding of bearing failures in slider–crank mechanisms and provides valuable insights for designing reliable and long-lasting systems.

Keywords: vibrational analysis; ball bearing; needle bearing; slider–crank mechanism; frequency analysis

MSC: 35A24; 65D25; 65F18; 74H15

Citation: Ghazwani, M.H.; Pham, V.V. Investigating Behavior of Slider–Crank Mechanisms with Bearing Failures Using Vibration Analysis Techniques. *Mathematics* **2024**, *12*, 544. https://doi.org/10.3390/math12040544

Academic Editors: Maria Luminița Scutaru, Catalin I. Pruncu and Luciano Lamberti

Received: 7 January 2024
Revised: 5 February 2024
Accepted: 7 February 2024
Published: 9 February 2024

1. Introduction

The slider–crank mechanism is one of the most versatile and common assemblies in machines. It is a four-bar chain mechanism with one sliding joint and three revolute joints. Pumps, compressors, internal combustion engines, quick return mechanisms, punches, etc., are some inversions of slider–crank mechanisms. The slider–crank mechanism converts rotational motion into linear motion. The motion of the slider–crank mechanism is possible due to the free movement of the revolute joints held together by bearings. These components are designed to have a long life without any failures. This mechanism supports various loads and allows relative motions among the crank, connecting rod, and slider. Therefore, bearings used in the mechanism undergo cyclic loading; as a result, they have a high chance of failure. There are two types of failure with a high probability of occurrence: cracks in parts containing bearings like races or cages and surface failures like abrasive wear, corrosive wear, pitting, and scoring. For this reason, many studies have been conducted to analyze the failures in vibration signature analyses of bearings. A detailed literature survey on failures in bearings is summarized below.

Butler [1] used the shock pulse method to detect damage in ball bearings, for which a stethoscope or any listening stick was used to listen to the shock pulses of damaged bearings. Gupta [2,3] analyzed the dynamics of cylindrical rolling element bearing. An analytical formulation for the rolling element bearing and the interaction of the rolling

element races with normal and moment vectors were proposed. The electro-hydrodynamic traction model was considered to calculate the roller race tractive forces during this analysis. Toersen [4] presented an experiment on damaged bearings and implemented an envelope technique to detect defects in ball bearings. The experimental results revealed that the defects depend upon the speed of the bearing corresponding to the frequency of the impact in the outer race, inner race, and ball uniquely. Mcfadden and Smith [5] developed a model to explain the vibrations caused by a single point defect in a bearing caused by a constant radial load. An impulse caused by a single point defect was considered an impulse function. The effect of the impulse function can be controlled by changing the magnitude of the impulse function. As the rolling elements roll over the defects, it causes an impulse with a fixed frequency in the bearing. The frequency depends on various parameters like bearing geometry, shaft speed, bearing load distribution, and location. When an impulse is generated in the bearing due to the defect, it creates a resonance between the bearing and the machine part to which it is fixed.

Patil et al. [6] presented research on localized bearing defects. The bearing was assumed to be a nonlinear spring, and the input force was considered a contact force whose calculations are carried out using Hertzian contact theory. The defect was assumed as a half-sine wave in which several readings are taken for different defect sizes and at various speeds. Vibration data were acquired in the time-domain signal and further converted into the frequency domain by fast Fourier transform analysis to find the exact resonance frequency. Tandon and Choudhury [7] proposed an analytical model for calculating the frequency and amplitudes of localized bearing under radial and axial bearing loads. For the inner race defect, sidebands were found around the peaks. The effect of load and pulse shape was also considered in the model and predicted that the magnitude of amplitude for the outer race is higher than that of the inner race. Liu et al. [8] developed a dynamic simulation model to study the effect of localized bearing defects, considering it as a two-degree-of-freedom system using piecewise functions and the Hertzian contact mechanism. The research found that it is essential to establish a relationship between impulse response and the defect's shape and size for its operation in a bearing. Choudhury and Tandon [9] have conducted several experiments using both good and defective bearings. An acoustic emission technique was applied to detect the roller bearing defect and compare the measured acoustic signals to find the flaws. Rubini and Meneghetti [10] presented a paper on applying envelope and wavelet transform analysis for fault diagnosis. The bearing defects can be analyzed by spectral analysis in classical vibrational analysis; however, this becomes very difficult if the forcing function is deficient.

Kiral and Karagulle [11] proposed a novel technique to use computer programming to perform the vibration response using a finite element analysis by applying a forcing function. The time and frequency domain analyses could be performed for healthy and damaged conditions followed by a comparison of the results to identify the exact cause of failures. Rai and Mohanty [12] applied the fast Fourier transform (FFT) of intrinsic mode functions in the Hilbert–Huang transform (HHT) technique to determine the failures in the bearing. Discrete Fourier transform and wavelet transform are beneficial for identifying the defect of bearings. Lu et al. [13] presented a paper on the fault diagnosis of motor bearings under variable speed using angular resampling of transient sound signals (TSA). A transient signal analysis tool was used to find the defect in the bearings; however, it is not a popular nor correct method for variable speed in a bearing analysis. Cui et al. [14] established a nonlinear vibration analysis technique to diagnose severe faults in bearings. The defect size is controlled in the outer race of the bearing; vibration signals are simulated and then analyzed for the defect impacts whose time interval gives the impact characteristics. Patel et al. [15] developed a dynamic model for vibration studies for deep-groove ball bearings with defects in multiple inner and outer races. In the analysis, the masses of the shaft, housing, races, and balls in their modelling are considered a parameter that influences the vibration characteristics. Salunkhe et al. [16] presented a study to analyze the vibration of deep-groove ball bearing using finite element analysis (FEA) and the

dimension analysis technique (DAT). Experimental work was performed to investigate the vibration characteristics of ball bearings. The FEA, DAT, and experiment results show that vibration amplitude is a critical function of surface fault size. Their study was found to be effective in estimating vibration amplitude and defect frequency within reasonable error. Nan et al. [17] improved a new model to investigate the dynamic analysis of a rolling ball-bearing rotor. Hou et al. [18] presented a comparative study using an acoustic emission and vibration analysis for the bearing fault diagnosis of high-speed trains. Their research was the first to compare the effectiveness of applying acoustic emission (AE) and vibration methods to diagnose a naturally degraded high-speed train bearing. Abdulbary et al. [19] analyzed fault diagnosis in a rotating system based on vibration analysis. Their goal of was to assist researchers in implementing identification, diagnosis, and repair techniques of common fault types using vibration analysis. Several fundamental techniques were provided for the condition monitoring of rotating systems, including fast Fourier transform, the frequency domain decomposition method, wavelet transform, stochastic subspace identification, and deep learning. Xiao et al. [20] developed a computational framework to investigate the fault-clearing failure mechanism of a reciprocating compressor system, and ADAMS software (version 2013.3) is used to create a simulation model of the mechanism. Jangra [21] listed a summary of the many gearbox issues and the methods used to diagnose them using vibration. The equipment was subjected to various loads, and the environment might cause deterioration. Many failures were detected by the methods used.

The present research contributed to understanding the internal dynamic mechanism of the rolling ball bearing and needle ball bearing through simulations which are practically helpful for predicting the impeding faults in rolling ball and needle bearings. This paper highlighted the mathematical equation analyses of the ball and needle ball bearings, which were further solved using MATLAB programming. In order to verify the mathematical results, experimental investigations were conducted using a vibration monitoring technique on the crank–chain mechanism. Further, small cracks were induced, and variations in vibration parameters such as amplitude and frequencies were observed concluded.

2. Mathematical Model

2.1. System Modeling for the Ball Bearings

Each ball bearing was assumed to be a nonlinear spring-mass damper system during analysis. The inner race of the bearing was connected to the shaft, and the outer race was kept fixed. A constant radial load was applied to the bearings. It was also presumed that the forces were applied when there was contact between the rolling element and the races. The differential equations are formed, and computer programs are written to solve them.

The forces which arise due to the contact of rolling elements with the races can be given as

$$F = k\delta^n \tag{1}$$

where F is the contact force, k is the Hertzian load deflection factor, δ is the deflection, and n is the exponent whose value is 3/2 for the ball bearing and 10/9 for the roller bearing. The value of k, i.e., Hertzian load factor, is calculated to be $7.0701 \times 10^9 \mathrm{N/m}^{3/2}$. A cross-section of the bearing with different parameters is shown in Figure 1.

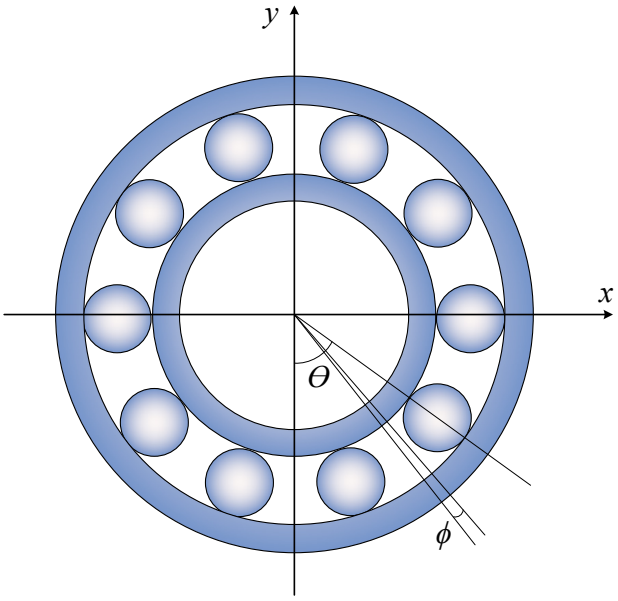

Figure 1. Cross-section of bearing showing different parameters.

2.2. Calculating the Forces

Using the Hertzian contact stress, we can calculate the forces applied by the individual ball on the races.

$$F = k[xcos(\theta_i) + ysin(\theta_i) - Cr]^{3/2} \tag{2}$$

where x is the displacement in the x direction, y is the displacement in the y direction, and θ_i is the angular position of the i-th bearing. This force can be resolved into x and y components for all the bearings as follows:

$$Fx = \sum_{i=1}^{z} k[xcos(\theta_i) + ysin(\theta_i) - Cr]^{3/2}\cos(\theta i) \tag{3}$$

$$Fy = \sum_{i=1}^{z} k[xcos(\theta_i) + ysin(\theta_i) - Cr]^{3/2}\sin(\theta i) \tag{4}$$

Now the defect for the inner and outer race is modeled as a sine function. The forces which arise in the defect region are as given as below

$$FFdx = \sum_{i=1}^{z} k\left[xcos(\theta_i) + ysin(\theta_i) - \left(Cr - Hd\sin\left(\frac{\pi}{\varphi}(\theta t - \theta i)\right)\right)\right]^{3/2}\cos(\theta i) \tag{5}$$

$$FFdy = \sum_{i=1}^{z} k\left[xcos(\theta_i) + ysin(\theta_i) - \left(Cr - Hd\sin\left(\frac{\pi}{\varphi}(\theta t - \theta i)\right)\right)\right]^{3/2}\sin(\theta i) \tag{6}$$

where

$$\varphi = \frac{Defect\ size}{Raceway\ size} \tag{7}$$

and for the inner race defect, φ yields

$$\theta t = \omega_c t + \frac{2\pi}{z(z-i)} \tag{8}$$

and for outer race defect

$$\theta t = (\omega_c - \omega)t + \frac{2\pi}{z(z-i)} \tag{9}$$

For the ball defect

$$\theta t = (\omega_b/z)t + \frac{2\pi}{z(z-i)} \tag{10}$$

where i depend on the number of defects. When the rolling elements are not in the defect region, the equations of motion are given as

$$m\ddot{x} + c\dot{x} + Fx = w \tag{11}$$

$$m\ddot{x} + c\dot{x} + Fy = 0 \tag{12}$$

When the rolling elements are in the defect region, the equations of motion are

$$m\ddot{x} + c\dot{x} + Fdx = w \tag{13}$$

$$m\ddot{x} + c\dot{x} + Fdy = 0 \tag{14}$$

where m is mass of the race based on which forces are to be calculated, c is the damping coefficient, and w is the load on the bearing.

2.3. MATLAB Program to Determine the State Variables for Roller Bearings

The MATLAB program (MATLAB R2018b) consists of two parts: one of them is the main program which calculates each time interval and stores the data, and the other is a function that solves the force equations. The differential equations are solved using the built-in function, ODE45, which uses a fourth-order Ranga–Kutta numerical differential approach. For the program, the following algorithm, as shown in Figure 2, was used. The parameters used in the program for all ball bearings are given Table 1.

Table 1. Specifications of the for ball bearing under investigation.

Quantities	Values
Hertzian contact load	7.0701×10^9 N/m^2
Radial clearance	20.5×10^{-6} m
Radial load	19.62 N
Damping coefficient	200 Ns/m
Mass of outer race	0.058 kg
For inner race	
Shaft speed	298 rpm = 31.2064 rad/s
Relative cage speed $(\omega_c - \omega_s)$	11.6292 rad/s
Length of defect	1 mm
Angular length of defect	71.942×10^{-3} rad
Height of defect	26.3890×10^{-3} mm
For outer race	
Shaft speed	304 rpm
Cage speed (ω_c)	11.8634 rad/s
Length of defect	2 mm
Angular length of defect	85.470×10^{-3} mm
Height of defect	106.456×10^{-3} mm
For rolling element	
Shaft speed	300 rpm
Cage speed (ω_b/z)	8.2391 rad/s
Length of defect	1 mm
Average angular length of defect	57.3387×10^{-3} rad
Height of defect	26.389×10^{-3} mm
Initial displacement in x	10^{-6} m
Initial velocity in x	0 m/s
Initial displacement in y	10^{-6} m
Initial velocity in y	0 m/s
Time for simulation	0–0.7 s
Time step	10^{-4} s

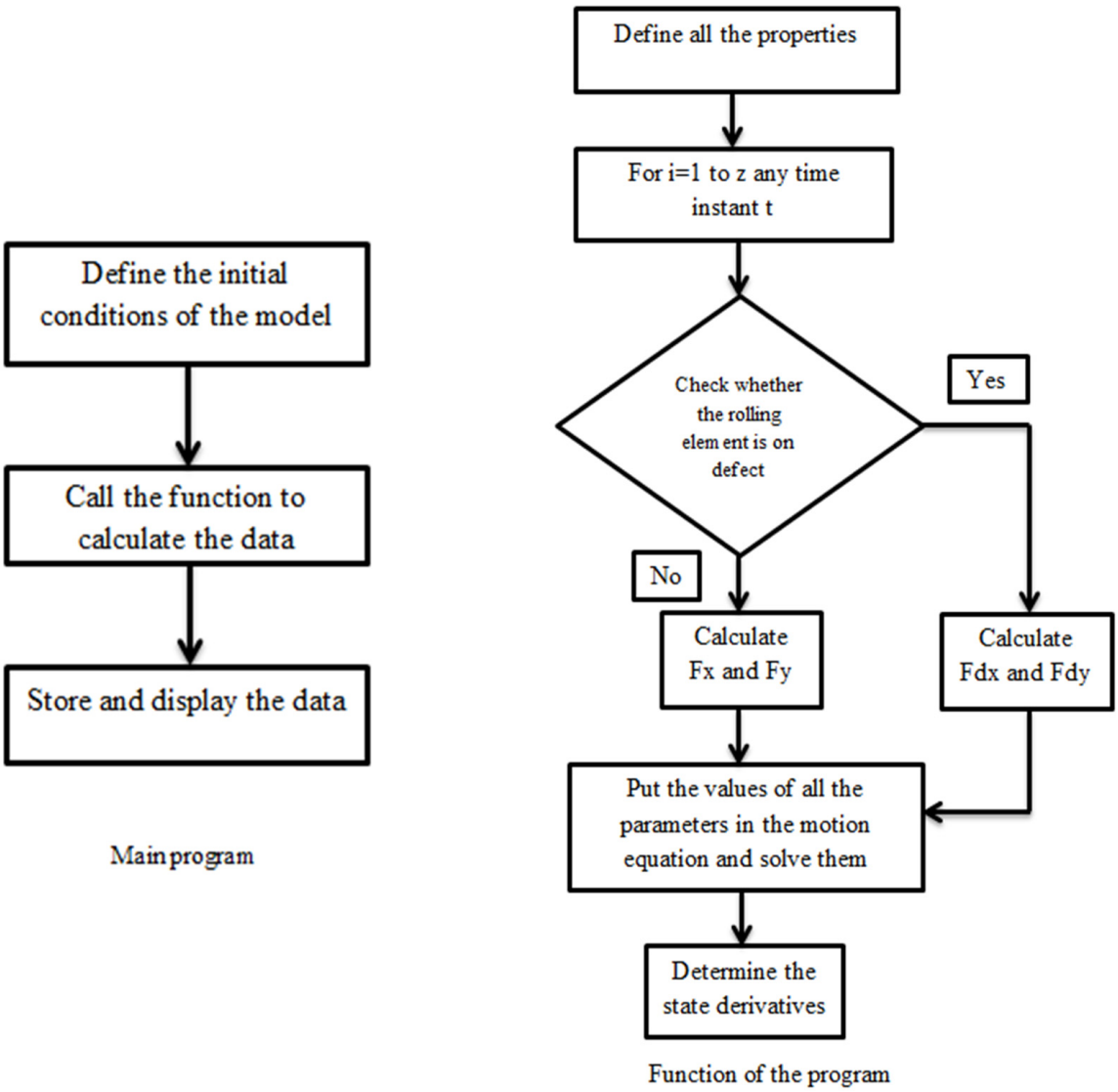

Figure 2. Algorithm to calculate state variables.

2.4. System Modeling for the Roller Bearings

The method described below is applied for the fault diagnosis of the needle roller bearing. It is located at the connection of the crank pin and connecting rod. The motion of the bearing is cyclic. A line defect has been induced in the pin and the connecting rod for the fault diagnosis. As the rolling elements roll over the defect, it generates an point of impact. The inter-impact time interval changes through a crank rotation, but the angle between the two defects remains constant. The inter-impact time is calculated for this analysis, and the frequency range is found. This range is relatively small for the crank pin defect compared to the defect on the connecting rod. Since the frequency range for the connecting rod defect is high, only the high- and low-frequency components are found.

2.5. The MATLAB Program to Determine the Frequency Range

Figure 3 shows how the MATLAB program (MATLAB 2018b) calculates the frequency, and the parameters used are given in Table 2.

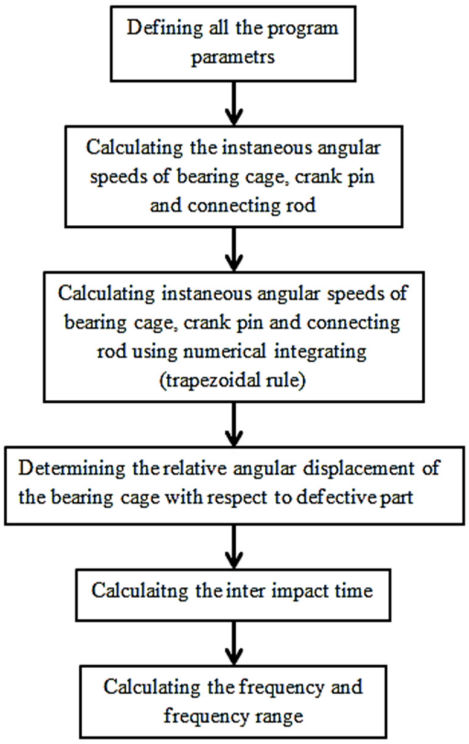

Figure 3. Algorithm to calculate frequency range.

Table 2. Parameters used to calculate the frequency range of bearing.

Quantity	Values
Crank radius	24.5 mm
Connection rod length	94 m
Rolling element diameter	2.5 mm
Pitch diameter	27.5 m
Number of rolling element	20
Inter-impact angular distance	0.314159265
Shaft speed for crack pin defect	314 rpm
Shaft speed for connecting rod defect	313 rpm

3. Experimental Setup

The experimental setup consists of a slider–crank mechanism obtained from a 100cc bike engine (Victor Enterprise, Kalamazoo, MI, USA). It contains two types of bearings, namely ball and needle bearings. Experimental work has been carried out on both of them. To support the deep crankshaft groove, ball bearings have been used to facilitate revolutions between the crank pin and connecting rod. Defects are induced at different locations of the bearings and evaluated for their diagnosis. The following are the parts that have been used to construct the setup.

3.1. Experiment Equipment

I. Engine block: Figure 4 shows the engine block used in this study. The piston slides on the cylinder of the engine block. The dimensions of the cylinder in the engine block are 5 cm in diameter and 9 cm in length.

Figure 4. Engine block.

II. Crank, connecting rod, and piston: The crank, the connecting rod, and the piston help to convert the reciprocating motion to rotational motion, as shown in Figure 5. One end of the connecting rod is connected at a length of 2.5 cm from the center of the crank, thus giving it a stroke length of 5 cm. With the connecting rod, the piston is attached with the help of a piston pin. The diameter of the piston is 4.9 cm, thus giving an actual swept volume of approximately 100 cm^3.

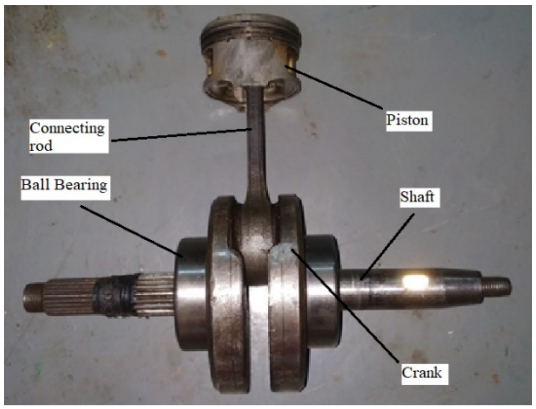

Figure 5. Crank, connecting rod, and piston.

III. Bearings: Each of the two ball bearings supports the two ends of the crankshaft. Bearings are used between the crank pin and the connecting rod to transfer the load torque from the piston to the crankshaft needle roller, as illustrated in Figure 6.

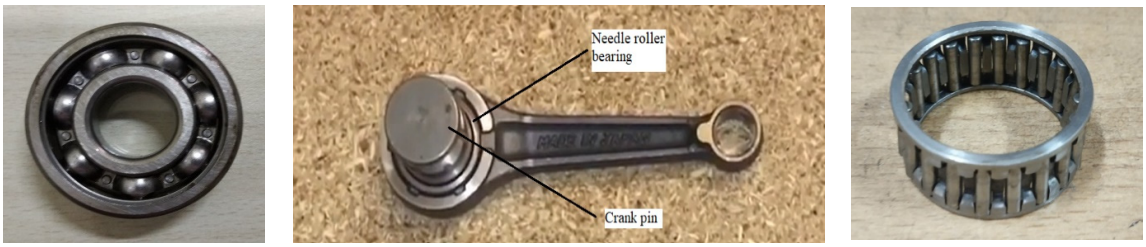

(**a**) (**b**) (**c**)

Figure 6. The construction of connecting rod: (**a**) ball bearing, (**b**) needle roller bearing between crank pin and connecting rod, and (**c**) ball bearing.

IV. Motor, gear, and pinion: An electric motor provides the motion in this setup. The whole setup is run with the help of a 220 volt, 3A ac motor (SMK0A-3A, Kalamazoo, USA).

The maximum rated rpm is 1400. A voltage regulator is attached to the motor to control the speed of the motor. For practical running purposes, the motor runs at 1200 rpm. A gear and pinion mechanism has been used to transmit the motion from the engine to the crank. The gear and pinion's pitch circle diameter are 64 mm and 16 mm, respectively, thus giving a gear ratio of 4. Though the rpm fluctuates from observation to observation, it stays around 300 rpm for most trials.

V. Stand and Frame: A frame and a stand are constructed to hold all the parts together.

3.2. Experimental Procedure

Five deep-groove ball bearings, SKF 6304, (VEXTA, Kalamazoo, USA) were used in this experiment. Among them, two are without any defects, and the rest have defects on the inner race, outer trace, and ball, respectively. Since the cage is permanently joined, there was no other way to access the inner race, balls, and outer race. So, the bearings had to be dismantled and then joined again. Similarly, to make observations on the defects in the needle roller bearing K 25 × 30 × 14, defects were induced in the pin and the connecting rod, and then observations are taken simultaneously.

3.3. Inducing Damage

Various methods were used to induce defects inside each part of the experiment. A hand-operated cutting tool was used to induce defects in the inner race. The width of the defect is about 2 mm. Figure 7 shows the defect in the inner race. Figure 8 shows the bearing with the outer race defect. The defect in the outer race was induced using a welding machine.

Figure 7. Inner race defect.

Figure 8. Outer race defect.

For the ball, the defect was induced with a hand tool, as illustrated in Figure 8. The defect's width is about 2 mm.

A wire EDM machine was used to induce a defect in the crank pin and connecting rod, as presented in Figure 9. The defect's width is 0.5 mm and is across the length of the crank pin and connecting rod.

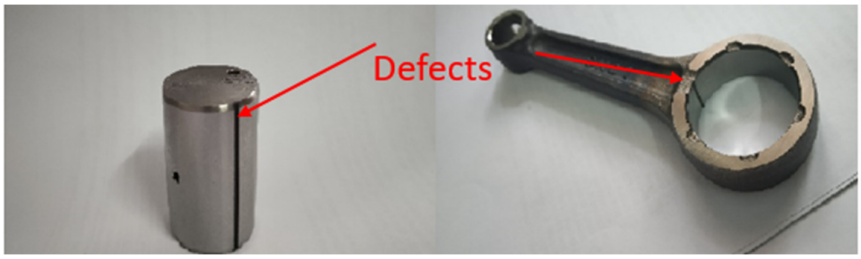

Figure 9. Crank pin and connecting rod defect.

3.4. Data Acquisition and Accelerometer

The vibrational data acquisition is performed using a PRUFTECHNIK VibXpert 2 (PRUFTECHNIK, Kalamazoo, USA) channel FFT analyzer and is recorded on Omnitrend software (OMNITREND2.5.0). Table 3 summarizes the vibration signal characteristics observed using the VibXpert analyzer (PRUFTECHNIK, Kalamazoo, USA) during test.

Table 3. Signal characteristics used in VibXpert analyzer during experiment.

Setup Class	Bearing Spectrum
Quantity	Acceleration
HP/LP Filter	1000/40,000
Frequency	400 Hz
Line No.	800
Window	Hanning
Envelope	On
Averages	3 (Linear)

A complete test setup with an VibXpert FFT analyzer, an accelerometer for acquiring the vibration data, and a laser tachometer used for measuring the rpm of the crankshaft, as shown in Figure 10.

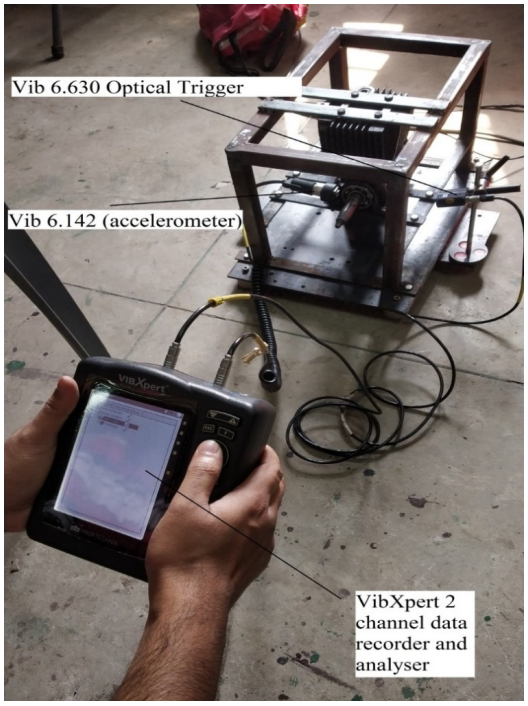

Figure 10. Experimental setup with accelerometer and laser stroboscope.

The acceleration transducer, VIB 6.142 DEX (FLUKE, Kalamazoo, USA), was mounted on bearing housings using a magnetic base. The specifications of the transducer (accelerometer), as given by OEM, are as follows: sensitivity, 1 mA/ms^{-2}; frequency range, from 1 Hz to 20,000 Hz; and resonance frequencies, about 360,000 Hz. The signals are collected using a VibXpert analyzer and analyzed using FFT. The corresponding signal peak is then calculated and matched with the experimental value.

4. Results and Discussions

4.1. Results for the Analysis of Defect in Ball Bearing

After solving the nonlinear differential equations, the radial displacement is obtained. The displacement vs. time plot obtained after running the simulation is given below. All the parameters are given in Table 1. The simulation was run for 0.7 s with a time step of 4–10 s, providing a good graph resolution.

The time between any two peaks was calculated to determine the defect frequency. Figure 11 represents the time for the second and third peaks, which was calculated to be 0.0474 s and 0.0932 s, respectively. The difference between the time intervals comes out to be 0.0458 s. The inverse of this time gives us the defect frequency, which is given as:

$$\frac{1}{T} = \frac{1}{0.0458\ \text{s}} = 21.83\ \text{Hz} \tag{15}$$

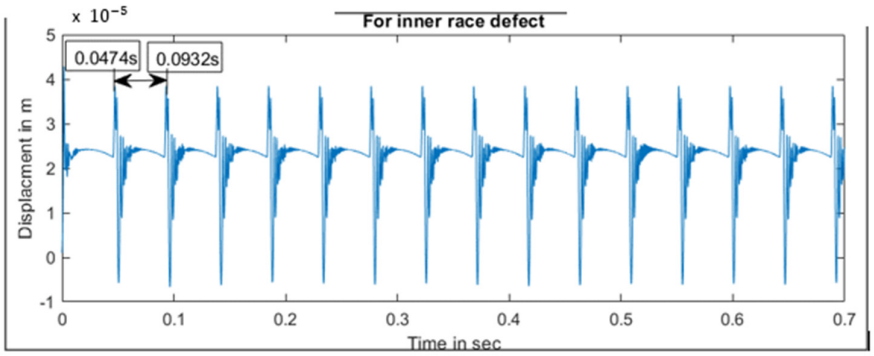

Figure 11. Displacement vs. time for inner race defect for ball bearing.

The experimental value for the defect as measured from the detector and the acceleration vs. frequency is plotted in Figure 12. As shown, the fundamental frequency for the inner race defects is 21.5 Hz. Additionally, the harmonics appear at 43 Hz. The balls enter and leave the defective region, causing deflections. In the load zone, the amplitudes of the impacts are the highest. They are reduced as the defect leaves the load zone.

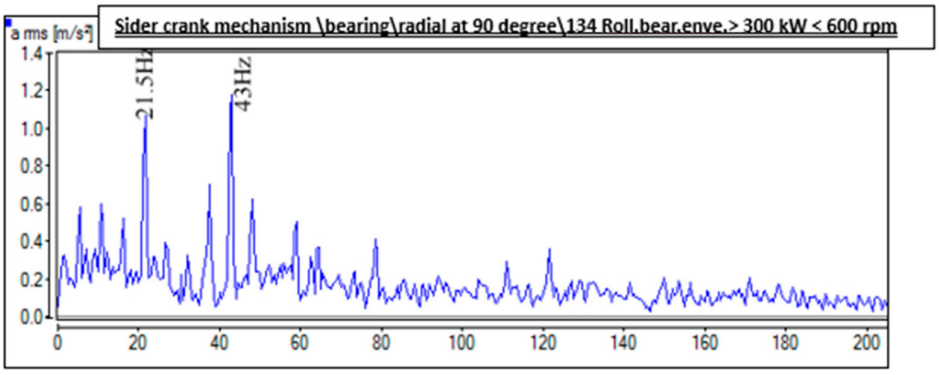

Figure 12. FFT spectra of inner race defect bearing for ball bearing.

Similarly, the displacement versus time data for the outer race defect of the ball bearing are plotted in Figure 13 using the nonlinear differential equations for the outer race. The time between any two peaks was again calculated to find out the defect frequency.

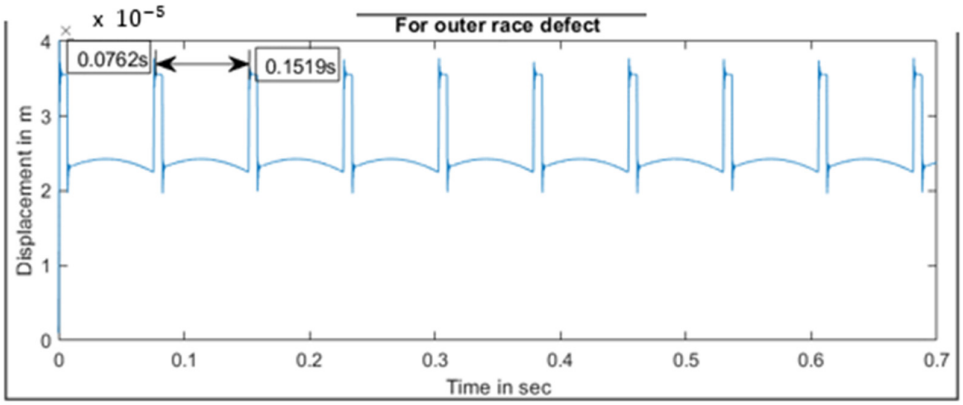

Figure 13. Displacement vs. time for outer race defect for ball bearing.

It can be seen that the time for the second and third peaks is 0.0762 s and 0.1519 s, respectively. The difference between the time intervals comes out to be 0.0757 s. The inverse of this time is the defect frequency, which is

$$\frac{1}{0.0757\ \text{s}} = 13.21\ \text{Hz} \tag{16}$$

The experimental value of the acceleration vs. frequency data of the outer race defect, as measured from the detector, is given in Figure 14. The fundamental frequency for the inner race defect is 13 Hz, and the harmonic appears at 26 Hz.

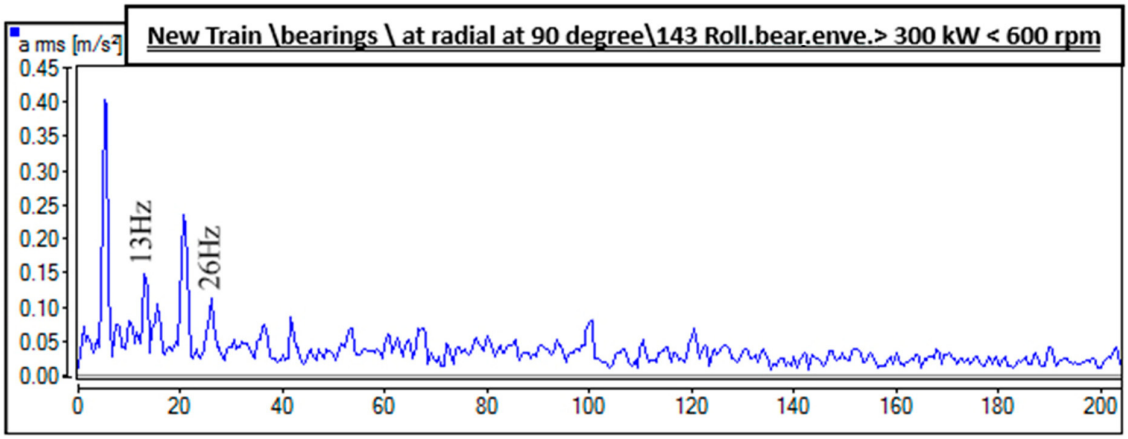

Figure 14. FFT spectrum of outer race defect bearing for ball bearing.

By solving the nonlinear differential equations for the ball bearing defect, the plotted in Figure 15 is obtained.

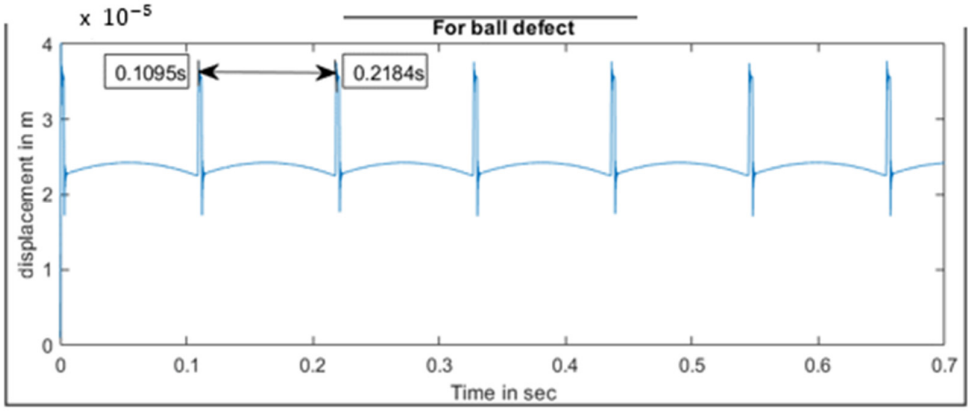

Figure 15. Displacement vs. time for ball race defect for ball bearing.

The time between any two peaks was again calculated to determine the defect frequency. Figure 15 shows that the time for the second and third peaks is 0.1095 s and 0.2184 s, respectively. The difference between the time intervals comes out to be 0.1089 s. The inverse of this time gives the defect frequency, which is

$$\frac{1}{0.1089\ \text{s}} = 9.18\ \text{Hz} \tag{17}$$

The experimental value of the acceleration versus frequency data of the outer race defect, as measured from the detector, is represented in Figure 16. The fundamental frequency for the inner race defect is 9.5 Hz, and the harmonics occur at 19 Hz.

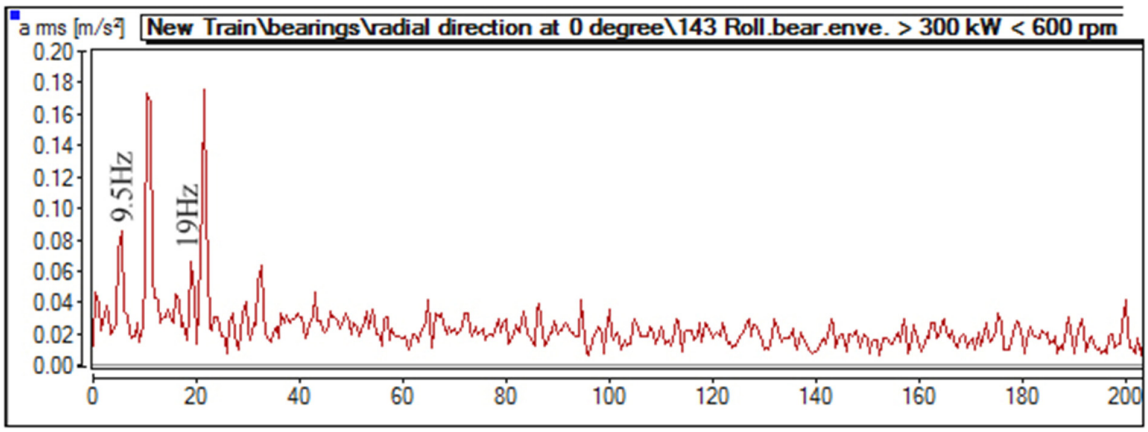

Figure 16. Spectrum of ball bearing.

4.2. Results for the Analysis of Defects of Needle Roller Bearing

After running the MATLAB code in Section 2.5, the frequency range is first calculated for the defect induced in the needle roller bearing. This is achieved by calculating the inter-impact time and then the frequency. Observations from the healthy bearing given in Figure 17 are also added for comparison.

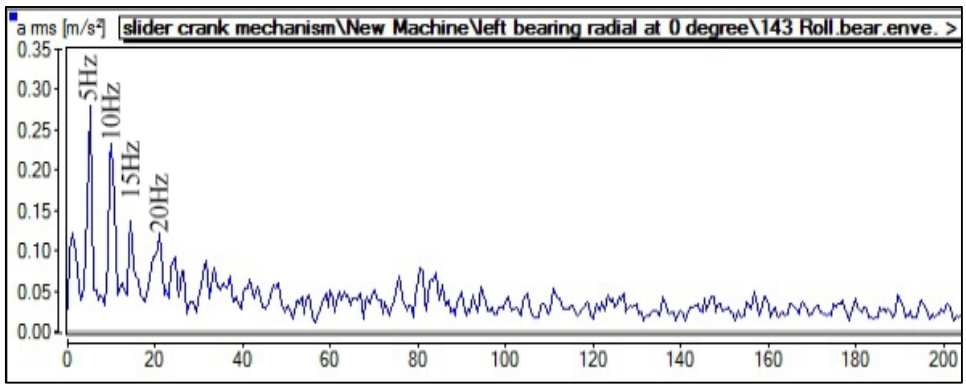

Figure 17. Spectrum of healthy ball bearing.

While the bearing runs at 5 Hz, the spectrum spike is seen at 5 Hz, and the harmonics of the fundamental vibrations are also visible at 10 Hz, 15 Hz, and 20 Hz. This may have arisen due to looseness in the bearing.

Figure 18 shows the FFT spectrum of the pin defect in the needle roller bearing. For the defect induced in the pin, the frequency range comes out to be between 137 and 167 Hz.

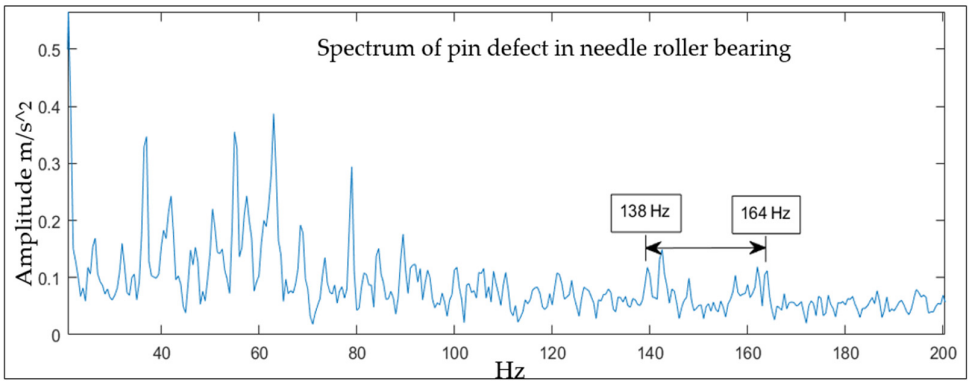

Figure 18. Spectrum of pin defect in needle roller bearing.

From the obtained data, relatively higher amplitudes are seen between 138 Hz and 164 Hz. The amplitudes appeared to be not very high because the accelerometer is attached to the ball bearing housing and not directly above the defective parts.

For the defect induced in the connecting rod, the frequency range comes out to be between 14 Hz and 82 Hz, as shown in Figure 19. Since the frequency range is high, it is complicated to predict the frequency components due to the defect in the connecting rod. Therefore, the extreme frequency components are only shown.

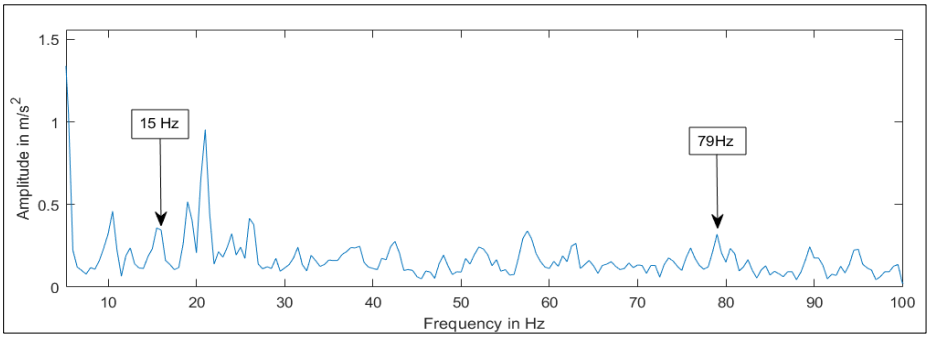

Figure 19. Spectrum of connecting defect in needle roller bearing.

From the result, the fault frequencies were calculated, which have been tabulated in Table 4. It can be noted that the calculated and the actual value of ball defect frequency was found to be varying because of the slippage of the rolling element within the races.

Table 4. Comparison of experimental and calculated data (Inner race defect Vs. Outer race defect Vs. Ball defect).

Defect Types	Calculated Defective Operating Frequency	Experimental Frequency
Inner race defect	21.83 Hz	21.5 Hz
Outer race defect	13.21 Hz	13 Hz
Ball defect	9.18 Hz	9.5 Hz

The motion of the bearing is cyclic, and a range of fault frequencies was computed instead of a single frequency. A straightforward approach to determine the fault frequency was proposed. This was based on inter-impact time when the rolling element rolls over the fault. To calculate the frequency range, a MATLAB program was written. The findings are summarized in Table 5.

Table 5. Comparison of experimental and calculated data (Pin defect Vs. Connecting rod defect).

Defect Types	Calculated Defective Frequency Range	Experimental Defective Frequency Range
Pin defect	137–167 Hz	138–164 Hz
Connecting rod defect	14–82 Hz	15–79 Hz

5. Conclusions

For the ball bearing, a mathematical model was developed. The bearing was modeled as a set of nonlinear spring-mass damper systems. The forces arising from the contact between the rolling element and the races were modeled using Hertzian contact theory.

The study was aimed to diagnose the impeding faults at the crank pin and the connecting rod in which the ball and needle roller bearings are used. The motion of the bearing is cyclic, and a range of fault frequencies was computed instead of a single frequency. A straight forward algorithm was proposed to determine the fault frequency. The experimental vibration data in terms of the spectra were used to identify the fault frequencies. Both theoretical and test results were compared with the healthy bearings. The average values of the vibration amplitude for the defective bearing was observed to be much higher than those of the healthy one for the same frequency range. Further, for the defect in the crank pin, the frequency range was small, and therefore, a range of fault frequencies was seen. The frequency range was high for the defect in the connecting rod; therefore, only the extreme frequencies were shown. The amplitude was minimal as the detector was not attached directly over the part containing the fault but to the ball bearing housing attached over the shaft.

Author Contributions: Conceptualization, methodology, software, validation, formal analysis, and investigation, M.H.G. and V.V.P.; resources, data curation, and writing—original draft preparation, M.H.G.; writing—review and editing, visualization, supervision, and project administration, M.H.G. and V.V.P.; funding acquisition, M.H.G. All authors have read and agreed to the published version of the manuscript.

Funding: The authors extend their appreciation to the Deputyship for Research & Innovation, Ministry of Education in Saudi Arabia, for funding this research work through project number ISP23-69.

Data Availability Statement: All data were included in this study. Data sharing is not applicable to this article.

Acknowledgments: The authors extend their appreciation to the Deputyship for Research & Innovation, Ministry of Education in Saudi Arabia, for funding this research work through project number ISP23-69.

Conflicts of Interest: The authors declare no conflicts of interest.

References

1. Butler, D.E. The Shock-pulse method for the detection of damaged rolling bearings. *Non-Destr. Test.* **1973**, *6*, 92–95. [CrossRef]
2. Gupta, P.K. Dynamics of rolling-element bearings part I: Cylindrical roller bearing analysis discussion. *J. Tribol.* **1979**, *101*, 293–302. [CrossRef]
3. Gupta, P.K. Dynamics of Rolling Element Bearings—2. Cylindrical Roller Bearing Results. *Am. Soc. Mech. Eng.* **1978**, *101*, 305–311. [CrossRef]
4. Toersen, H. Application of an envelope technique in the detection of ball bearing defects in a laboratory experiment. *TriboTest* **1998**, *4*, 297–308. [CrossRef]
5. McFadden, P.D.; Smith, J.D. Model for the vibration produced by a single point defect in a rolling element bearing. *J. Sound Vib.* **1984**, *96*, 69–82. [CrossRef]
6. Patil, M.S.; Mathew, J.; Rajendrakumar, P.K.; Desai, S. A theoretical model to predict the effect of localized defect on vibrations associated with ball bearing. *Int. J. Mech. Sci.* **2010**, *52*, 1193–1201. [CrossRef]
7. Tandon, N.; Choudhury, A. An analytical model for the prediction of the vibration response of rolling element bearings due to a localized defect. *J. Sound Vib.* **1997**, *205*, 275–292. [CrossRef]
8. Liu, J.; Shao, Y.; Lim, T.C. Vibration analysis of ball bearings with a localized defect applying piecewise response function. *Mech. Mach. Theory* **2012**, *56*, 156–169. [CrossRef]
9. Choudhury, A.; Tandon, N. Application of acoustic emission technique for the detection of defects in rolling element bearings. *Tribol. Int.* **2000**, *33*, 39–45. [CrossRef]
10. Rubini, R.; Meneghetti, U. Application of the envelope and wavelet transform analyses for the diagnosis of incipient faults in ball bearings. *Mech. Syst. Signal Process.* **2001**, *15*, 287–302. [CrossRef]
11. Kiral, Z.; Karagülle, H. Simulation and analysis of vibration signals generated by rolling element bearing with defects. *Tribol. Int.* **2003**, *36*, 667–678. [CrossRef]
12. Rai, V.K.; Mohanty, A.R. Bearing fault diagnosis using FFT of intrinsic mode functions in Hilbert-Huang transform. *Mech. Syst. Signal Process.* **2007**, *21*, 2607–2615. [CrossRef]
13. Lu, S.; Wang, X.; He, Q.; Liu, F.; Liu, Y. Fault diagnosis of motor bearing with speed fluctuation via angular resampling of transient sound signals. *J. Sound Vib.* **2016**, *385*, 16–32. [CrossRef]
14. Cui, L.; Zhang, Y.; Zhang, F.; Zhang, J.; Lee, S. Vibration response mechanism of faulty outer race rolling element bearings for quantitative analysis. *J. Sound Vib.* **2016**, *364*, 67–76. [CrossRef]
15. Patel, V.N.; Tandon, N.; Pandey, R.K. Dynamic model for vibration studies of deep groove ball bearings considering single and multiple defects in races. *J. Tribol.* **2010**, *132*, 041101. [CrossRef]
16. Salunkhe, V.G.; Desavale, R.G.; Kumbhar, S.G. Vibration Analysis of Deep Groove Ball Bearing Using Finite Element Analysis and Dimension Analysis. *J. Tribol.* **2022**, *144*, 081202. [CrossRef]
17. Nan, G.; Jiang, S.; Yu, D. Dynamic analysis of rolling ball bearing-rotor based on a new improved model. *SN Appl. Sci.* **2022**, *4*, 173. [CrossRef]
18. Hou, D.; Qi, H.; Luo, H.; Wang, C.; Yang, J. Comparative study on the use of acoustic emission and vibration analyses for the bearing fault diagnosis of high-speed trains. *Struct. Health Monit.* **2022**, *21*, 1518–1540. [CrossRef]
19. AbdulBary, M.; Embaby, A.; Gomaa, F. Fault Diagnosis in Rotating System Based on Vibration Analysis. *ERJ. Eng. Res. J.* **2021**, *44*, 285–294. [CrossRef]
20. Xiao, S.; Xiao, Q.; Song, M.; Zhang, Z. Dynamic analysis for a reciprocating compressor system with clearance fault. *Appl. Sci.* **2021**, *11*, 1295. [CrossRef]
21. Jangra, D. A Review on Different Faults in Gearbox and Vibration Based Diagnosis. *Int. J. Curr. Eng. Technol.* **2022**, *12*, 315–325. [CrossRef]